ISSN 2319-5991 www.ijerst.com

Peer Reviewed, Referred & Indexed Journal

Research Paper

Intelligent ANN-Based Control of a Bridgeless PFC On-Board Charger with Compact DC-Link for Electric Vehicles

Dr. K. Srinivas[1], B. Cherishma[2]

[1]Professor, Department of Electrical and Electronics Engineering, JNTUH University College of Engineering (Autonomous) Jagtial ,Telangana, India.

[2] PG, M.Tech (Electrical Power Systems), Department of Electrical and Electronics Engineering, JNTUH University College of Engineering (Autonomous) Jagtial ,Telangana, India.

Abstract: ***Onboard charging infrastructure has to be efficient, small, and strong to keep up with the demands of an expanding fleet of electric cars. This research aims to shed light on a new method for controlling a small electric vehicle on-board charger (OBC) that use a bridgeless PFC system. An acronym for "Artificial Neural Networks," the tactic is dependent on them. The suggested design does away with the conventional diode bridge rectifier to boost system efficiency and cut down on conduction losses. Regardless of the situation, the ANN controller keeps the DC-link voltage low, the input current form near unity, and the total harmonic distortion (THD) low. Among the many benefits of the compact DC-link design are increased power density, enhanced system dependability, and a reduced footprint for passive components. The improved control technique outperforms the state-of-the-art in three key areas: efficiency, dynamic responsiveness, and conformity with power quality criteria, according to robust MATLAB/Simulink simulations. In light of these findings, the suggested ANN-controlled bridgeless PFC OBC may be considered for inclusion in upgraded electric vehicle charging stations in the near future.***

Keywords_ Electric Vehicles (EVs), on-board chargers, intelligent control, compact DC-link, big efficiency, nonlinear control systems, unity power factor, harmonic mitigation, and total harmonic distortion (THD).

I. INTRODUCTION

Electric vehicle (EV) sales continue to rise every year, driven by rising demand for cleaner, more efficient, and less expensive modes of transportation [1]. Powering anything from rickshaws to automobiles, electric vehicles rely on batteries. Efficient onboard chargers (OBCs) are especially important for eRickshaw drivers during rush hour because of their busy schedules [2]. A number of people are looking at using tiny yet effective single-phase integrated OBCs to meet these demands [3]. The referenced integrated OBC is a good illustration of this [4]. It charges electric vehicles directly from a single-phase power supply using two inverters. Easily connected to the grid and vehicles, a DC onboard charger is detailed in both [5] and [6]. With the addition of fast-charging capabilities and additional powertrain technologies, the later surpasses the former. While integrated charger designs have several advantages over simpler chargers that rely on single-phase AC-DC converters, they often need more complex hardware and control methods. To address issues like control complexity and power imbalance, researchers have examined several topologies. Tan et al. [7] proposed a three-tiered quick charger as a solution to the

voltage imbalance in neutral-point-clamped (NPC) converters. The integration of a non-isolated buck DC-DC stage with an unregulated resonant AC-DC converter was made easier by Lee et al. [9]. Studies on efficient methods of charging many automobiles simultaneously have also focused on reducing superfluous power processing via the use of AC-DC converters [10]. Electric car chargers cannot be considered PQ compliant only based on their fast charging capability. Numerous AC-DC PFC converters, some using bridgeless topologies and others depending on the more conventional diode bridge rectifiers, have been developed for use in electric car charging applications [11]. Canonical switching cell (CSC), Cuk, Zeta, SEPIC, and Luo topologies of PFC converters were all thoroughly examined by Singh et al. [12]. The many benefits of bridgeless AC-DC converters are leading to their rising popularity [13], [14]. These benefits include higher efficiency, lower conduction losses, and enhanced power density. Although it increases the system's complexity and component count, traditional bridgeless systems often include separate converter legs for the positive and negative half cycles [13], [15], [16]. Conventional, one-stage slow charger designs based on bridgeless Zeta and Cuk, respectively, are shown in Figure 1(a) [15] and Figure 1(b) [16]. It is important to maintain tight control over the charging process and power factor correction (PFC) in one-stage devices. Partition the AC-DC and DC-DC stages,
correspondingly, in two-stage systems. Despite offering greater control possibilities, two-stage systems do come with a few significant drawbacks. The slower charging and increased number of front-end components cause them to have a lower power density and less efficiency [16]. High power density electric car chargers are compatible with many current PFC topologies, as shown in [17].

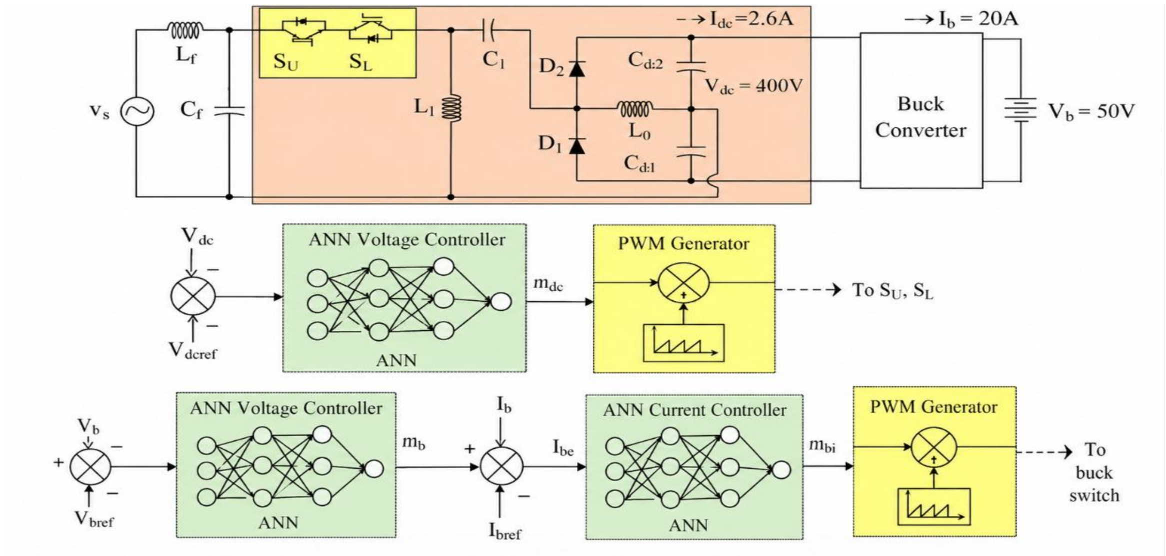

Fig.1 On-Board Charger Configuration.

There is an urgent demand for compact, efficient, and reliable on-board charging solutions since the electric vehicle industry is developing. Despite their simplicity of manufacture and high efficiency, typical single-stage AC-DC converters-particularly those based on buck-boost topologies-require a large DC-link capacitance, which is a significant disadvantage. Consequently, despite their size, reliability concerns, higher space needs, and low power density, electrolytic capacitors are often used. The paper propose a method for controlling a bridgeless Zeta PFC onboard charger (OBC) that uses an ANN-based high-voltage compact DC-link design to potentially circumvent these drawbacks. With less conduction losses, the device outperforms the conventional diode bridge rectifier. In addition to reducing component count and stress on the switch voltage, the bridgeless Zeta design makes use of components across both half cycles of the AC supply.Using a higher DC-link voltage (400 V) to run the PFC stage, which significantly reduces the required DC-link capacitance, is an original part of this study. The square of the DC-link voltage is inversely proportional to capacitance, which is why this is the case. Thus, dependable film capacitors may replace cumbersome electrolytic capacitors, resulting in higher power density and extended system life.

An ANN-based controller adjusts the input current and DC-link voltage to boost efficiency. The ANN controller achieves low total harmonic distortion (THD) and a power factor near to unity regardless of the input voltage or load, because to its greater flexibility compared to typical PI controllers. Operating in discontinuous conduction mode (DCM), the system streamlines control implementation by removing complex sensing and phase-locked loop (PLL) procedures. The proposed technique accomplishes CC-CV battery charging by using a cascaded buck converter stage and a high DC-link voltage, as opposed to utilising low DC-link voltages (such as 65 V to charge a 48 V battery at 0.1C). The improved power transmission capabilities of this setup allow for charging rates that are eight times faster than those of traditional sluggish chargers.

II. SYSTEM CONFIGURATION AND OPERATION

The system configuration is show in fig.1 The current coming into the onboard battery charger is controlled by the new BL Zeta converter, The fact that each half-cycle operation needed two sets of converter cells indicates that the early BL Zeta converters probably had a high component count. A two-way switch (S) and two very fast diodes (D_1 and D_2) are the only components of the suggested charger. L_i, L_o, and C_i, the transfer capacitor, do not change throughout either the positive or negative half cycles. The output split capacitor of this design lowers the switch voltage stress to $V_{in}+V_{dc}/2$, as opposed to the usual $V_{in}+V_{dc}$ voltage used by the regular BL Zeta converter. By running the PFC converter at a higher DC-link voltage, the suggested setup outperforms single-stage EV chargers [15]. Since DC-link capacitance is inversely proportional to output voltage, running the Zeta converter at a higher DC-link voltage results in a lower DC-link capacitance. Hence, low power chargers might employ film capacitors instead of the large electrolytic capacitors since they are smaller and more reliable. This section will describe the proposed BL Zeta converter in depth, including its three modes of operation: switchON, switchOFF, and DCM period. Diagrams 2(a)-(d) show these modes. When starting the BL Zeta converter in Mode-I, the bidirectional switch's top device and bottom body diode are both switched on. At this time, current is not flowing via diode D1. Fig.2(a) and (d) demonstrate that two inductors, Lo and Li, begin charging in order to store the energy. The second stage buck converter receives its current from two DC-link capacitors, C_{dc1} and C_{dc2}.Fig.3(d) shows the waveforms of the voltage and current, which are important in this mode.

$$V_{Li} = L_i\frac{diLi}{dt} = V_{in}(t);\ V_{Lo} = L_o\frac{diLo}{dt} = V_{in}(t) \quad (1)$$

$$i_{SU} = i_{SL} = i_{Li} + i_{Lo};i_{D1} = i_{D2}=0 \quad (2)$$

$$i_{Li}(t) = \frac{Vin}{Li}t_{on} + I_{Li\,min} \quad (3)$$

$$i_{Lo}(t) = \frac{Vin}{Lo}t_{on} + I_{Lo\,min} \quad (4)$$

The input inductor's voltage (V_{Li}) and current (i_{Li}) are represented by these symbols. Likewise, V_{Lo} and i_{Lo} represent the voltage and current, respectively, at the output inductor. The second step of mode II is to put the diode D_2 into conduction and turn off the upper switch SU. Once the inductors L_i release the energy from the capacitor C_i, the charging process may commence. Fig.2(b) shows that throughout this time, C_{dc2} continues to discharge, while C_{dc1} charges thanks to the energy transferred from L_o. The following equations characterise the switching waveforms for the inductor and capacitor voltages, as seen in Fig. 2(d).

$$V_{Li} = V_{in}(t) - V_{dc}/2;\ \ V_{Lo} = V_{in}(t) - V_{dc}/2$$

$$i_{SU,L} = 0;\ \ i_{D1,2} = i_{Li} + i_{Lo}$$

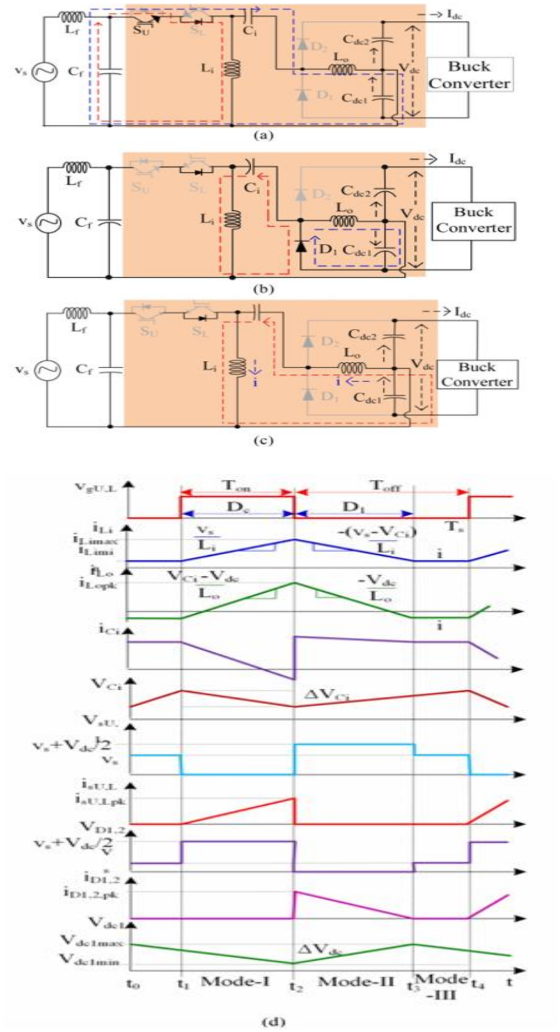

Fig.2 Operation of BL PFC converter: (a) mode-I: Switch ON period, (b) mode-II: switch OFF period, and (c) mode-III: DCM period (d) switching waveforms over one Ts of positive line cycle

$$i_{Li}(t) = \frac{Vin}{Li} - \frac{Vdc}{2Li} t_{off} + I_{Li\,max} \quad (5)$$

$$i_{Lo}(t) = \frac{Vin}{Lo} - \frac{Vdc}{2Lo} t_{off} + I_{Lo\,max} \quad (6)$$

When tonnage = dT_s, we may get the input inductor current ILimax and the output inductor current $I_{Lo1,2max}$, where V_{dc} is the DC-link voltage of the BLSI Cuk converter. At the end of stage II, using equations (14) and (15), these currents are approximated at $t_{off} = (1\text{-}d\text{-}d_1)T_s$. The length of stage III, abbreviated as DCM, is 1 in this case. In step three, also called mode III, a current of the same magnitude flows in the opposite direction of the output inductor, analogous to what happens when conduction of diode D_1 is terminated. As seen in Fig.2(c), the converter undergoes a phase transition upon stopping.

There is a simultaneous supply of current to the load from the two output capacitors. Three modes-low switch, high switch body diode, and diode D_2-are recognised even in a negative supply cycle. With the use of time intervals t_3 and t_4, we can measure how long the DCM lasts when no conducting device is present. You can find the relevant equations below, and Fig.2(d) displays the waveforms for the time interval t_2-t_3.

$$t_3 - t_4 = T_s - \{(t_2 - t_1) + (t_3 - t_2)\} \quad (7)$$

$$I_{dc} = V_{dc}/RL \quad (8)$$

Idc represents the DC-link current and RL stands for the effective resistive load of the BLSI Cuk converter.

Since $i_{Li}(t) + i_{Lo}(t) = 0$ for DCM, we may derive it from (14) and (15).

$$d_1T_s = \frac{2Vin}{Vdc} dT_s \quad (9)$$

The voltage gain M for this BL converter may be calculated using equation (18) and the condition, $dT_s + d_1T_s < T_s$.

$$\frac{Vdc}{Vin} = \frac{2D}{(1-D)} = M \quad (10)$$

III. CONTROL TECHNIQUE

High power density, lower DC-link capacitance, improved efficiency, quicker battery charging, power quality maintenance are all goals of the proposed onboard charger. Its two-stage design enables the control of both the grid-side and battery-side operations at the same time by means of a bridgeless Zeta PFC AC-DC converter and a buck DC-DC converter. The decreased DC-link capacitance needed when using the bridgeless Zeta converter is a result of its inverse square relationship with voltage, which allows it to function at greater DC-link voltages. Tiny, dependable film capacitors may boost power density and extend the life of the system, replacing bulky electrolytic capacitors.

Thanks to its built-in power factor adjustment, very low transient harmonic distortion (THD), and operation in discontinuous conduction mode (DCM), this converter is almost perfect. There is no need for current sensors or PLL synchronisation.
A simple PI-based voltage loop controls the PFC stage, while a cascaded voltage-current arrangement controls the buck converter. Because they are physically separated by the DC-link, the two converters will operate continuously and autonomously. Future electric vehicle in-car chargers should make use of this suggested technology due to its small size, mobility, efficiency, improved power quality, and quick charging time.

TABLE I

SYSTEM CHARGER SPECIFICATIONS WITH NEW BL ZETA CONVERTER

S. No	Specifications	New BL Zeta Converter	Buck Converter
1	Input voltage (V_s)	110V, Single-phase AC	400 V DC
2	Change in Output voltage/current (V_{dc}/I_{dc})	300V – 400V /2.6A	50V/20 A
3	Switching frequency (f_s)	20 kHz	50 kHz
4	Resonant frequency (f_r)	2 kHz	-
5	Output Power (P)	1 kW	-
6	Battery Rating	65V/26 Ah	-
7	Permissible Current Ripple in input inductor (δ)	20%	-
8	Permissible Voltage Ripple in DC-link capacitor(Δ)	3%	-
9	Permissible Voltage Ripple in Output capacitor (λ)	1%	-

TABLE II

SELECTION OF CIRCUIT COMPONENT FOR SYSTEM CHARGER

S. No.	Parameter	Design Expression	Calculated Value	Selected Value	Mode
1	Input Inductor (L_i)	$L_i=(V_{in}T_s / \delta I_{in}).(V_{dc} / (2V_{in}+V_{dc}))$	0.918 mH	1 mH	CCM
2	Equivalent Inductance (L_{eq})	$L_{eq}=(V_{in}^2V_{dc}^2T_s) / (4P(V_{dc}+2V_{in})^2)$	25 µH	25 µH	DCM
3	Output Inductance (L_o)	$L_o = L_iL_{eq} / (L_i - L_{eq})$	25 µH	25 µH	DCM
4	Transfer Capacitor (C_i)	$C_i = 1 / ((2\Pi f_r)^2(L_i – L_o))$	10 µF	10 µF	CCM
5	Filter Capacitance ($C_{f\ max}$)	$C_{fmax}=(P.\tan\theta) / (2\Pi f.V_s^2)$	2.75 µF	1.1 µF	-
6	Filter Inductor (L_f)	$L_f=[1/(4\Pi^2f_c^2C_f)]-[(.04.V_s^2)/(2\Pi f.P)]$	3.77 mH	4 mH	-
7	DC-Link Capacitor ($C_{dc1,2}$) ANN-based charger	$C_{dc1,2}=I_{dc}/(2*2\Pi f\Delta V_{dc})=P/(4\Pi fV_{dc}\Delta V_{dc})$	345 µF	400 µF	-

8	Buck Inductance (L_b)	$L_b \leq L_{bc} = (V_b(1-D_b)T_s)/(2I_b)$	130 µH	50 µH	DCM
9	Output Capacitor (C_b)	$C_b=(D_bV_b)/(f_{sw}(V_b^2/P)\lambda V_b)$	378 µF	400 µF	-

The suggested layout uses a lower DC-link capacitance while maintaining the same ripple voltage. The schematic of the on-board charger that has been suggested is seen in Fig.1. In contrast to the buck converter's cascade controller, this battery charging technique employs a voltage follower mechanism to keep the current and voltage constant. You won't need input side sensing or a PLL. Pulse width modulation (PWM) based on voltage feedback controls the PFC converter in direct current mode (DCM). In contrast, CC-CV mode uses dual loop PI control to manage the electric vehicle's battery current. Below are the output and error figures of two converter controllers at the nth sampling moment.

$$V_{dce}(n) = V_{dcref}(n) - V_{dc}(n) \quad (11)$$

$$mm_{BL}(n) = m_{BL}(n-1) + K_{pd}\{V_e(n) - V_e(n-1)\} + K_{id} \cdot V_e(n) \quad (12)$$

Find the voltage discrepancy between the desired DC link voltage (V_{dcref}) and the actual DC link voltage (V_{dc}) by using the output (m_{BL}) of the voltage controller, an integral constant (K_{id}), and a proportional constant (K_{pd}). The converter's switching frequency processes the control signal (m_{BL}) and an internally generated triangle wave (Sc) to create the following pulse sequence:

If $S_c < m_{BL}$, then $S_{U,L} = ON$

$$\text{Otherwise, } S_{U,L} = OFF \quad (13)$$

During charging, the $S_{U,L}$ switch regulates the necessary duty cycle in response to changes in input voltage; $S_{U,L}$ are the gate signals for this switch. That, basically, is the way that control and error signals are sent to a buck converter:

$$I_{be}(n) = I_{bref}(n) - I_b(n) \quad (14)$$

$$m_{bI}(n) = m_{bI}(n-1) + K_{pI}\{I_{be}(n) - I_{be}(n-1)\} + K_{iI} \cdot I_{be}(n) \quad (15)$$

$$V_{be}(n) = V_{bref}(n) - V_b(n) \quad (16)$$

$$m_{bV}(n) = m_{bV}(n-1) + K_{pV}\{V_{be}(n) - V_{be}(n-1)\} + K_{iV} \cdot V_{be}(n) \quad (17)$$

The voltage difference between the set and measured battery voltages (V_{bref} and V_b, respectively) is represented by a comparable set of variables: V_{be}, the proportional constant; K_{iV}, the integral constant; and m_{bV}, the voltage controller's output. At 80% state of charge (SOC), the battery may be charged.

V. ANN CONTROLLER

To regulate the converter's output current and voltage, an ANN-based controller is employed in place of PI controller. By comparing and contrasting input-output data from systems with different loads and grid configurations during training, artificial neural network(ANN) controllers may adapt to non-linear dynamics, setting them apart from traditional PI controllers. The system's control accuracy, responsiveness to changes in conditions, and power factor correction are all enhanced by this repair, which furthermore significantly lowers total harmonic distortion (THD). Using an ANN-based approach improves control of dual-battery charging, power sharing equity, and robust operating in short-term scenarios. To make the compensating device work better, an ANN controller with several back propagation layers is employed. We train the ANN using the MATLAB toolbox. Training the ANN controller using Levenberg-Marquardt-Backpropagation yields better results than using gradient-degressive or Gauss-Newton methods. The Levenberg-Marquardt back propagation method has several advantages, such as faster convergence, reduced memory requirements, and competent learning [9]. The standard PI controller's data set is the only one used to train the ANN. It is proposed that artificial neural networks be controlled using a controller with one output layer, 10 hidden layers, and two input levels. The ANN controller receives both the initial and revised error signals, which measure the difference between the actual and reference values in the d and q coordinate systems. The goal of an ANN controller should be to reduce error as much as possible without sacrificing precision. The ANN controller is responsible for transforming the dqo data into the ABC format. As shown in Figure 3, the mean square error, which is the discrepancy between the input and target values, is used to evaluate the performance of the ANN controller.

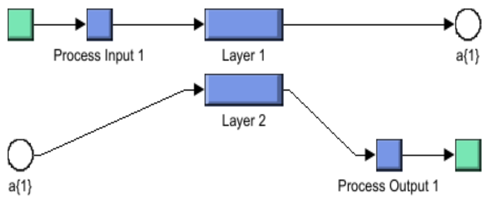

Fig.3 Typical Structure of ANN control

VI. SIMULATION RESULTS

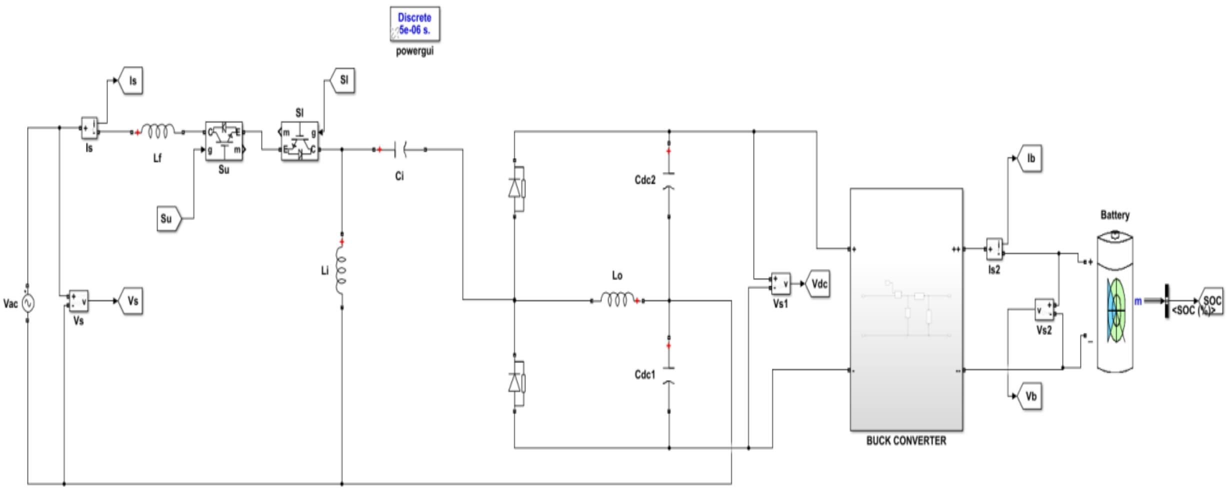

Fig.4 Schematic of the on-board charger based on BL Zeta converter using MATLAB/SIMULINK, which uses less components.

A) RESULTS WITH PI CONTROLLER

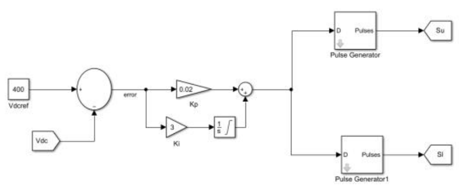

Fig.5 Control system for AC-DC Converter.

The above Fig.5 shows the PI-based control system for the AC-DC converter. It regulates the DC-link voltage by comparing the reference and actual voltage and generates PWM pulses to control the converter switches.

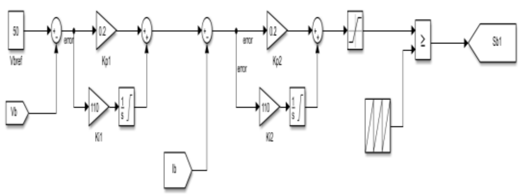

Fig.6 Control system for DC-DC Buck Converter.

The above Fig.6 shows the PI controller for the DC-DC buck converter. It regulates the battery charging voltage and current by generating PWM pulses, ensuring stable and efficient battery charging.

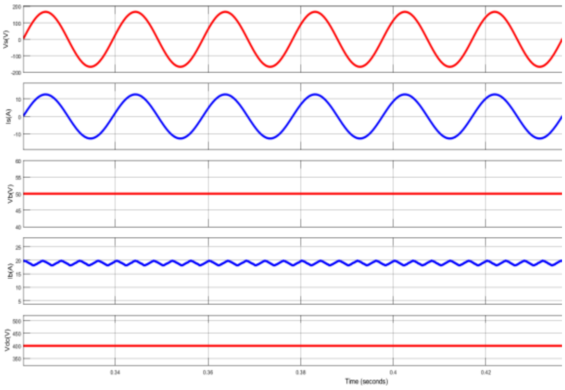

(a)

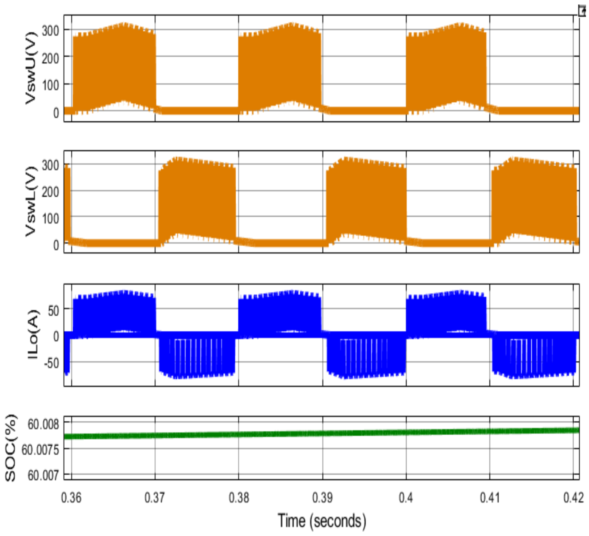

(b)

Fig.7 (a) Operation of on-board charger at rated line voltage steady state waveforms. (b) Switching operation.

The steady-state results confirm stable operation of the EV charger is shown in Fig.7(a). The source voltage and current remain sinusoidal and in phase, indicating a high power factor. The battery voltage (50 V), battery current (20 A), and DC-link voltage (400 V) stay constant, while the gradual increase in SOC confirms efficient and reliable battery charging.

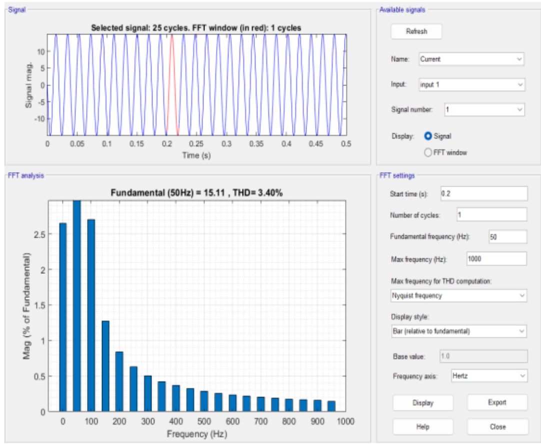

Fig.8 Operation of on-board charger at rated line voltage improved PQ indices.

The Fig.8 shows that the input current is nearly sinusoidal with a THD of 3.40%, which is below the IEEE-519 limit of 5%. The low harmonic content indicates good power quality, high power factor, and efficient operation of the proposed on-board charger.

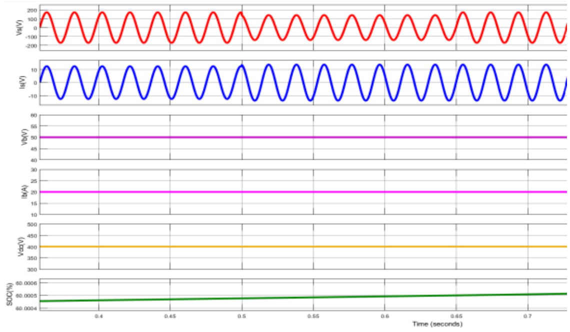

(a)

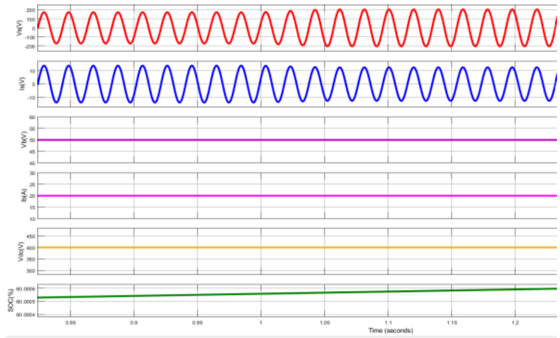

(b)

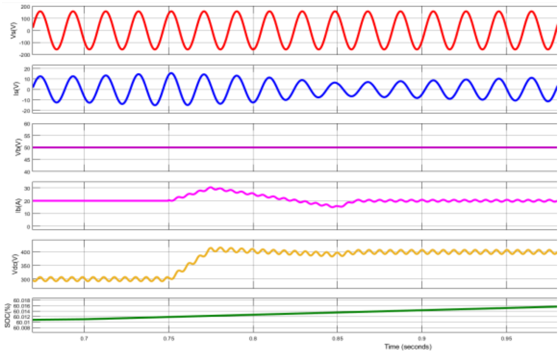

(c)

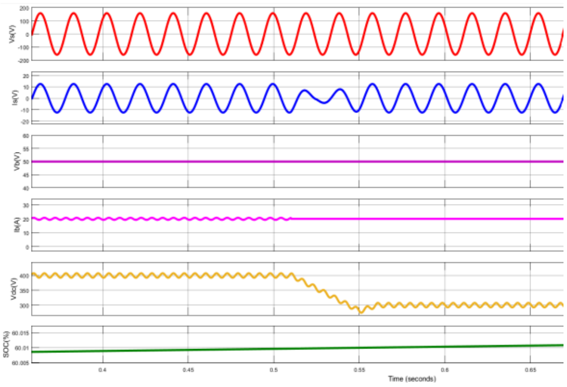

(d)

Fig.9 Transient performance of the on-board charger during line and DC-link voltage changes (a) from 110 V to 90 V, (b) from 110 V to 130 V, (c)from 300 V to 400V (d) from 400V to 300V.

The above Fig.9 shows the on-board EV charger operates stably under different conditions. The source voltage and current remain sinusoidal and in phase, indicating a high power factor, while the battery voltage (50 V), charging current (20 A), and DC-link voltage are well regulated. During disturbances, the controller quickly restores normal operation with only temporary variations, and the continuous increase in SOC confirms reliable and efficient battery charging.

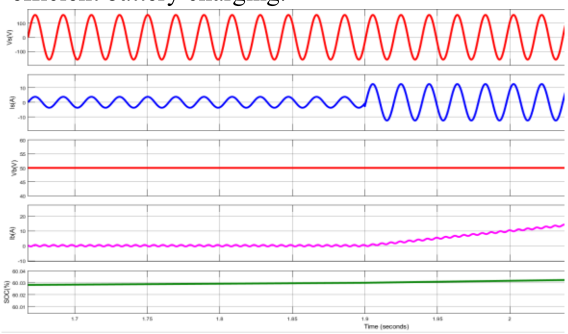

(a)

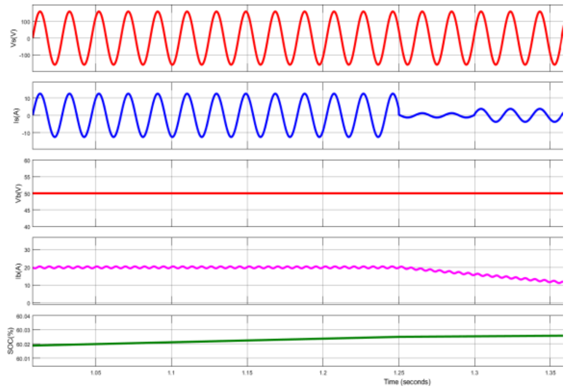

(b)

Fig.10 Transient Performance of charger. (a) during startup, and (b) shutdown process.

The above Fig.10 shows the EV charger responds effectively to changes in charging current. While the source voltage remains constant, the source and battery currents adjust smoothly to the charging demand. The battery voltage stays regulated at 50 V, and the gradual increase in SOC confirms stable and efficient battery charging.

B) RESULTS WITH ANN CONTROLLER

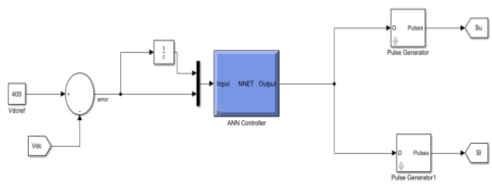

Fig.11 Control system for AC-DC Converter.

The above Fig.11 shows the ANN-based control of the AC-DC converter. It compares the reference and actual DC-link voltage, and the ANN generates PWM pulses for switches S_1 and S_2 to maintain a stable DC-link voltage with improved dynamic performance.

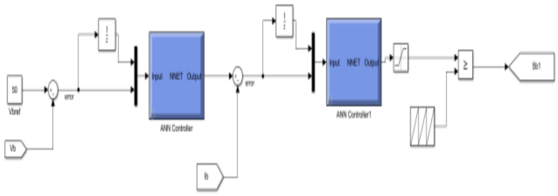

Fig.12 Control system for DC-DC Buck Converter.

The above Fig.12 shows the ANN-based control of the DC-DC buck converter. The ANN regulates the battery voltage and charging current by generating PWM pulses, providing faster response, lower ripple, and more efficient battery charging than a conventional PI controller.

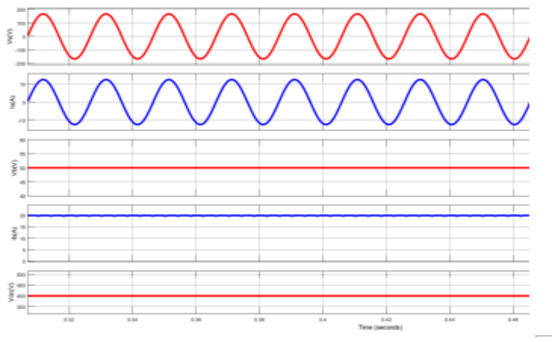

(a)

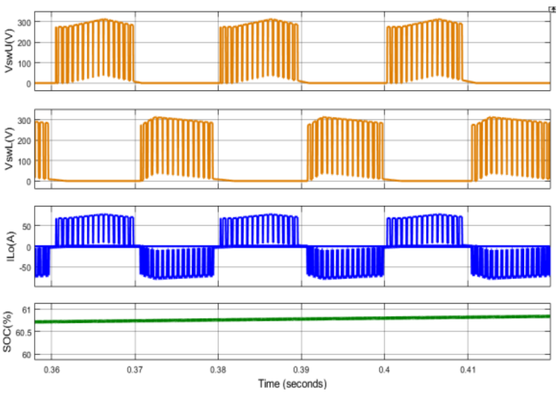

(b)

Fig.13 (a) Operation of on-board charger at rated line voltage steady state waveforms. (b) Switching operation.

The steady-state waveform confirms stable ANN-controlled charger operation is shown in Fig. 13. The source voltage and current remain sinusoidal and in phase, indicating effective power factor correction and near-unity power factor. The battery voltage is maintained at 50 V, the charging current at 20 A, and the DC-link voltage at 400 V with minimal fluctuations, ensuring efficient and reliable power transfer.

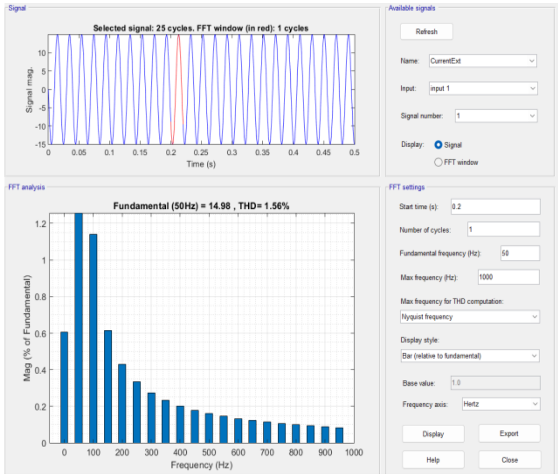

Fig.14 increased PQ indices while using the recommended on-board charger at the rated line voltage.

The above Fig.14 shows the input current closely follows the source voltage, achieving a near-unity power factor of 0.99 and a low THD of 1.56%. This demonstrates the ANN controller's effectiveness in reducing harmonics, improving power quality, minimizing losses, and ensuring efficient battery charging. m

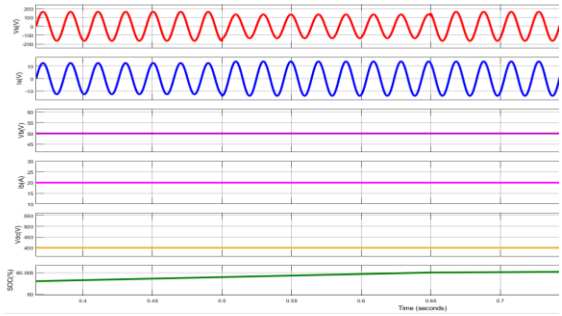

(a)

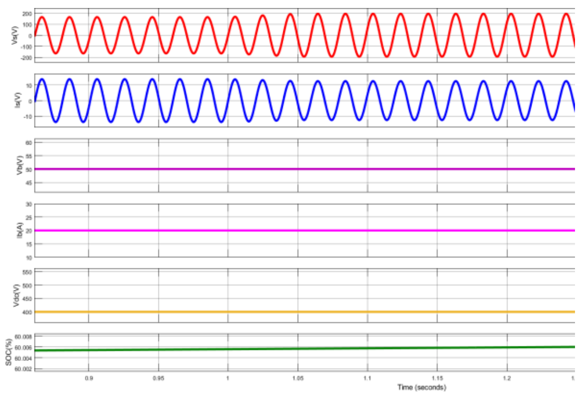

(b)

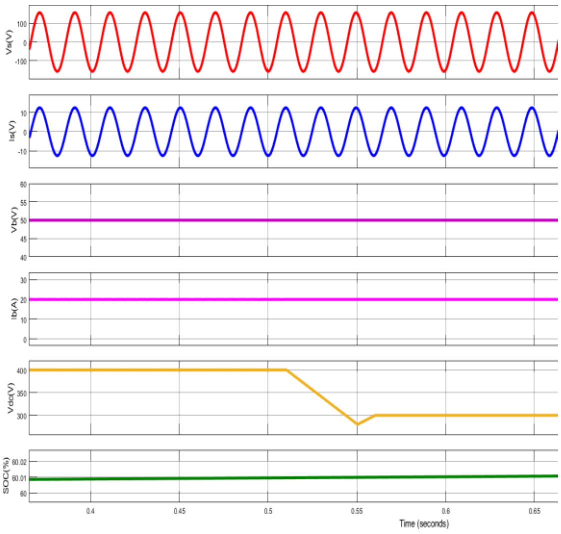

(c)

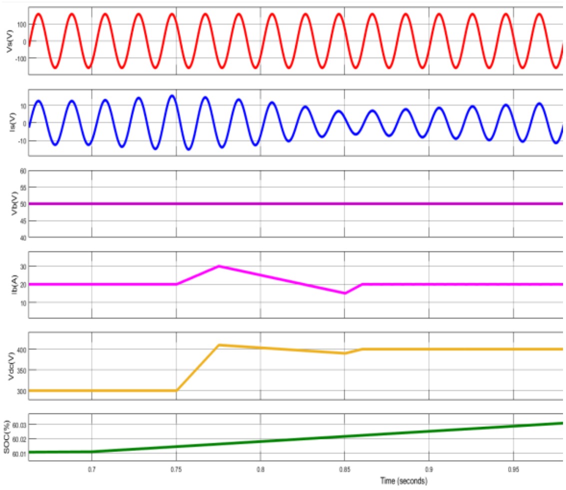

(d)

Fig.15 Transient performance of the on-board charger during line and DC-link voltage changes (a) from 110 V to 90 V, (b) from 110 V to 130 V, (c) from 300 V to 400 V, and (d) from 400 V to 300 V, illustrate the transient performance of the proposed on-board charger.

The above Fig.15 shows the ANN-controlled charger works well even when the input voltage or DC-link reference changes. The source current stays smooth and follows the source voltage, while the battery voltage (50 V), charging current (about 20 A), and DC-link voltage remain stable. The controller quickly adjusts to changes with very little fluctuation, ensuring continuous and reliable battery charging.

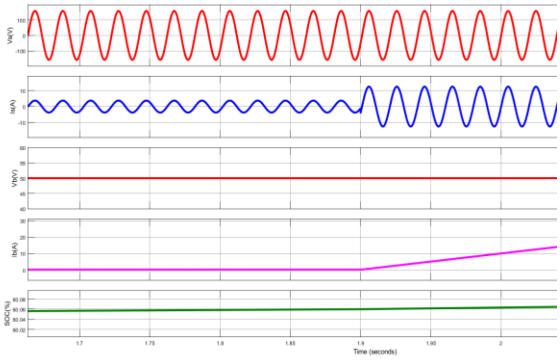

(a)

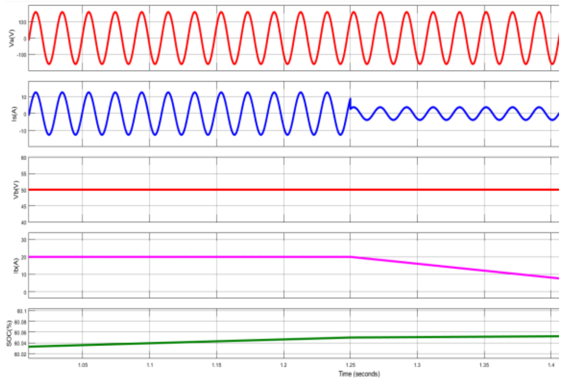

(b)

Fig.16 Transient Performance of charger. (a) during startup, and (b) shutdown process.

The startup and shutdown results, the smooth operation of the ANN-controlled charger shown in Fig.16. During startup, the source and battery currents increase gradually to their rated values, while during shutdown they decrease smoothly to zero. The battery voltage remains stable at 50 V throughout, ensuring reliable charging and controlled operation.

COMPARSION TABLE

Parameter	PI Controller	ANN Controller
Settling Time	0.25 – 0.35 sec	0.08 – 0.15 sec
Rise Time	0.15 sec	0.05 sec
Overshoot	8%	3%
Total Harmonic Distortion (THD)	3.46%	1.56%
Power Factor (PF)	0.95	0.99

Dynamic Response	Moderate	Fast
Transient Recovery Time	~0.3 sec	~0.1 sec
Efficiency	88% – 92%	94% – 97%
Control Complexity	Low	High
Adaptability	Fixed (needs tuning)	Self-adaptive (learning-based)
Performance under Disturbance	Moderate	Excellent

CONCLUSION

To enhance the overall performance of the system, this research introduces a novel bridgeless (BL) Zeta converter for onboard charging of electric vehicles (EVs). Intelligent control based on Artificial Neural Networks (ANNs) is used by the converter. With a low component count of only two diodes and two inductors, the proposed design achieves great component sharing throughout each half-cycle of operation, resulting in amazing efficiency and improved power density over the whole battery charging range. When compared to traditional slow chargers, operating at a higher DC-link voltage results in better thermal performance and system lifespan. This is because a dramatic decrease in the required DC-link capacitance enables the use of smaller and more reliable capacitors. By lowering the voltage stress on the switch, the proposed arrangement paves the way for less expensive and lower-rated semiconductor devices. The input current form, dynamic responsiveness, and DC-link voltage may be fine-tuned under a variety of scenarios by implementing an ANN controller. The system satisfies the prerequisites for power quality with a power factor near one and a total harmonic distortion (THD) level below one. According to the results, the proposed charger may charge batteries eight times faster than the existing norm, which is a huge improvement. Furthermore, the system maintains seamless operation while enhancing efficiency and decreasing losses. The proposed ANN-controlled BL Zeta converter offers a tiny, affordable, and intelligent onboard charging solution; it is ideal for use in next-gen electric cars that need fast charging, high-quality power, and improved dependability.

REFERENCES

[1] T. Esram and P. L. Chapman, "Comparison of photovoltaic array maximum power point tracking techniques," IEEE Trans. Energy Convers., vol. 22, no. 2, pp. 439–449, Jun. 2007.

[2] M. A. G. de Brito, L. P. Sampaio, G. A. Melo, and C. A. Canesin, "Main maximum power point tracking strategies for photovoltaic arrays," IEEE Trans. Ind. Electron., vol. 60, no. 3, pp. 1156–1167, Mar. 2013.

[3] B. Singh, B. N. Singh, A. Chandra, K. Al-Haddad, A. Pandey, and D. P. Kothari, "A review of single-phase improved power quality AC–DC converters," IEEE Trans. Ind. Electron., vol. 50, no. 5, pp. 962–981, Oct. 2003.

[4] J. Zhang, J. Shao, and J. Wu, "Review of power factor correction techniques in single-phase AC–DC converters," IEEE Access, vol. 7, pp. 120255–120269, 2019.

[5] S. Dusmez and A. Khaligh, "A compact and integrated multifunctional power electronic interface for plug-in electric vehicles," IEEE Trans. Power Electron., vol. 28, no. 12, pp. 5690–5701, Dec. 2013.

[6] H. H. Choi, "An improved bridgeless PFC converter with reduced conduction losses," IEEE Trans. Power Electron., vol. 29, no. 11, pp. 6006–6015, Nov. 2014.

[7] L. Huber and M. M. Jovanović, "Design-oriented analysis and performance evaluation of bridgeless PFC boost rectifiers," IEEE Trans. Power Electron., vol. 25, no. 1, pp. 85–94, Jan. 2010.

[8] B. Singh and S. Singh, "State of the art on power factor correction converters for electric vehicle chargers," IEEE Trans. Ind. Appl., vol. 52, no. 5, pp. 4213–4224, Sep./Oct. 2016.

[9] K. Yao, X. Ruan, X. Mao, and Z. Ye, "Improved bridgeless Zeta converter for PFC applications,"

IEEE Trans. Power Electron., vol. 26, no. 11, pp. 3139–3148, Nov. 2011.

[10] S. Singh and B. Singh, "A single-stage Zeta converter-based power factor corrected EV battery charger," IEEE Trans. Veh. Technol., vol. 66, no. 7, pp. 5535–5545, Jul. 2017.

[11] M. K. Kazimierczuk, Pulse-Width Modulated DC–DC Power Converters. Hoboken, NJ, USA: Wiley, 2015.

[12] N. Mohan, T. M. Undeland, and W. P. Robbins, Power Electronics: Converters, Applications, and Design, 3rd ed. Hoboken, NJ, USA: Wiley, 2003.

[13] R. W. Erickson and D. Maksimović, Fundamentals of Power Electronics, 2nd ed. Boston, MA, USA: Springer, 2001.

[14] S. Dusmez, A. Khaligh, and O. Hasanzadeh, "A novel integrated onboard charger for electric vehicles," IEEE Trans. Veh. Technol., vol. 64, no. 2, pp. 546–555, Feb. 2015.

[15] Y. Chen, X. Ruan, and H. Yan, "DC-link capacitor minimization in single-phase PFC converters," IEEE Trans. Power Electron., vol. 28, no. 1, pp. 452–462, Jan. 2013.

[16] J. Sun, "Small-signal methods for AC distributed power systems—A review," IEEE Trans. Power Electron., vol. 24, no. 11, pp. 2545–2554, Nov. 2009.

[17] H. Wang, F. Blaabjerg, and M. Liserre, "Reliability of power electronic systems for EV applications," IEEE Trans. Power Electron., vol. 28, no. 6, pp. 2975–2987, Jun. 2013.

[18] S. Bacha, I. Munteanu, and A. I. Bratcu, Power Electronic Converters Modeling and Control. London, U.K.: Springer, 2014.

[19] J. Liu, Y. Miura, and T. Ise, "Comparison of control methods for DC–DC converters in EV chargers," IEEE Trans. Power Electron., vol. 30, no. 4, pp. 2029–2040, Apr. 2015.